CHALMERS

Modeling Large Equipment Behavior in the Sea Splash-Zone Using Methods of Computational Fluid Dynamics

Master's thesis in Engineering Mathematics and Computational Science

TIMOFEY MUKHA

Department of Applied Mechanics
Division of Fluid Dynamics
CHALMERS UNIVERSITY OF TECHNOLOGY
Gothenburg, Sweden 2012
Master's thesis 2012:52

MASTER'S THESIS IN ENGINEERING MATHEMATICS AND COMPUTATIONAL SCIENCE

Modeling Large Equipment Behavior in the Sea Splash-Zone Using Methods of Computational Fluid Dynamics

TIMOFEY MUKHA

Department of Applied Mechanics
Division of Fluid Dynamics
CHALMERS UNIVERSITY OF TECHNOLOGY
Gothenburg, Sweden 2012

Modeling Large Equipment Behavior in the Sea Splash-Zone Using Methods of Computational Fluid Dynamics
TIMOFEY MUKHA

Master's thesis 2012:52
ISSN 1652-8557
Department of Applied Mechanics
Division of Fluid Dynamics
Chalmers University of Technology
SE-412 96 Gothenburg
Sweden
Telephone: +46 (0)31-772 1000

Chalmers Reproservice
Gothenburg, Sweden 2012

Modeling Large Equipment Behavior in the Sea Splash-Zone Using Methods of Computational Fluid Dynamics
Master's thesis in Engineering Mathematics and Computational Science
TIMOFEY MUKHA
Department of Applied Mechanics
Division of Fluid Dynamics
Chalmers University of Technology

Abstract

Oil industry uses a complex device, called the "Christmas tree" (XT in the remainder of the thesis) to control the hydrocarbon flow out of the oil well and for various other purposes. In case of off-shore extraction, the device has to be submerged into the water and then delivered further down. The most dangerous part of the delivery process is known to be the splash-zone of the sea.

In order to effectively simulate the XT's behaviour during delivery, a geometrically simplified model of the latter has to be created. Yet this model should posses the hydrodynamical properties of a real XT. In the first part of this thesis, a computational fluid dynamics (CFD) simulation is performed to investigate the results of a previous experimental work conducted on some proposed XT models. Significant disagreement between experimental results and the results of CFD modelling has been observed. Possible explanations of this divergence are given.

In the second part of this work the methodology of modelling the XT's behaviour in the splash-zone using CFD is developed. The built model allows to simulate different weather conditions and evaluate the forces acting on the XT. The necessity of including fluid-structure interaction (FSI) into the model is investigated by comparing results obtained with and without FSI respectively.

Keywords: Drag, Multiphase, VOF, FSI

Preface

This thesis deals with the development of a framework for modeling the behaviour of large equipment in the sea splash-zone using contemporary CAE software and numerical methods.

The sea splash-zone can be roughly defined as the space above the sea level where the equipment can be hit by violent water waves. Commonly equipment passes the splash-zone during its delivery to or from the sea bottom. Depending on the weather conditions the splash-zone may or may not be suitable for a piece of equipment to pass through it, because of the damage that large waves can deal. Determining the suitability of the weather conditions for conducting a delivery is a complicated task which could be assisted by computer modeling.

This work is divided into two parts, each dealing with a separate aspect of creating the aforementioned model. The first part focuses on the development of a substitute geometry for the "Christmas tree", which is a name for a piece of equipment used in hydrocarbon production. It plays a big role in the work of FMC Technologies, which interests are behind this thesis, and in the oil industry in general and is therefore given a special treatment. The substitute geometry is needed because using the original (very complex) geometry of the "Christmas tree" in the model would be very expensive in terms of computational resources.

The second part of the thesis focuses on modeling the splash-zone itself and the interaction between the waves and a potential piece of equipment, the latter being abstractly represented by a box. Complicated physics are in action in the splash-zone so many modeling aspects have to be considered such as multiphase flow and wave generation. Simulating the interaction of the waves and the equipment-box requires dealing with structural mechanics and setting up inter-solver communication which makes things even more intricate.

The outcome of the thesis is not a ready-to-use modeling framework. A much larger timeframe and more computing power is needed to bring this work to its final goal. However, the hope is that the results obtained here would serve as a good start up for those who pick up on the project at FMC Technologies.

Acknowledgements

Firstly I would like to thank Elias Bernerskog, manager of the CFD group at XDIN AB, for accepting me as a master thesis worker and doing everything to help me become a part of the CFD team at XDIN. I would also like to thank my supervisors Tobias Tivert from XDIN and Srdjan Sasic from Chalmers University of Technology for their enormous support and the many things they taught me about CFD and numerics. I am also grateful for the enthusiasm of Per Thomas Moe from FMC Technologies, which served as a great motivation for trying to bring this thesis to a high standard. Last but not least I would like to thank Tobias Berg from ANSYS for all his help with ANSYS Fluent.

Contents

Abstract i

Preface iii

Acknowledgements iii

Contents v

1 Introduction 1

2 Evaluating the Drag Force on an XT Model 2
2.1 Background, Outline and Goals . . . 2
2.2 The XT Model . . . 3
2.3 The Computational Domain . . . 4
2.3.1 Boundary conditions . . . 4
2.3.2 Initial Conditions . . . 5
2.4 The Computational Mesh . . . 5
2.4.1 The Surface Mesh on the Model . . . 5
2.4.2 The Volume Mesh . . . 6
2.5 Modelling the Fluid Flow . . . 8
2.5.1 Turbulence Modeling . . . 8
2.5.2 Solver Algorithm . . . 9
2.5.3 Discretization . . . 10
2.5.4 Solution Strategy . . . 10
2.6 Results . . . 10

3 Simulating the XT's Behaviour in the Splash-Zone 12
3.1 Outine and Goals . . . 12
3.2 The XT Model . . . 12
3.3 The Computational Domain . . . 12
3.3.1 Suitability for Wave Modeling . . . 12
3.3.2 Blockage Problem . . . 13
3.4 The Computational Mesh . . . 14
3.4.1 Mesh for the Fluid . . . 14
3.4.2 Mesh for the XT . . . 14
3.5 Boundary Conditions . . . 15
3.6 Modeling the Fluid Flow . . . 16
3.6.1 Generating Waves . . . 16
3.6.2 Turbulence Modeling . . . 17
3.6.3 Solver Algorithm . . . 18
3.6.4 Multiphase Flow Modeling . . . 18
3.6.5 Discretization . . . 18
3.7 Fluid-Structure Interaction . . . 19
3.7.1 FSI in ANSYS Workbench . . . 19
3.7.2 The System Coupling Service . . . 20
3.7.3 Data Transfer Algorithms . . . 20
3.7.4 Dynamic Meshing . . . 21
3.8 Initial Conditions . . . 21
3.9 Results . . . 22
3.9.1 Effect of Fluid-Structure Interaction . . . 26

4 Conclusions 28

5 Appendix **30**

1 Introduction

The creation of an oil well is a complicated multi-staged process. After the well is finally ready for production it is crowned by a device called the "Christmas tree" (XT in the remainder of the thesis). The XT is, roughly speaking, a complicated collection of valves and spools. The main function of the XT is controlling the flow of hydrocarbons out of the well.

The peculiar name of the device originates from the visual similarity between earlier XTs and an actual tree. A picture of a XT is shown on figure 1.0.1.

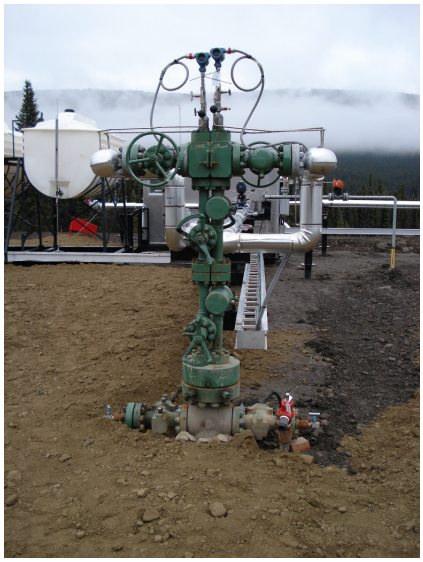

Figure 1.0.1: *An example of a XT.*

However when working in a subsea environment the XT has to be placed in a metal frame and the resemblance is lost completely. A drawing of a modern version of the device used by FMC Technologies is shown on figure 1.0.2.

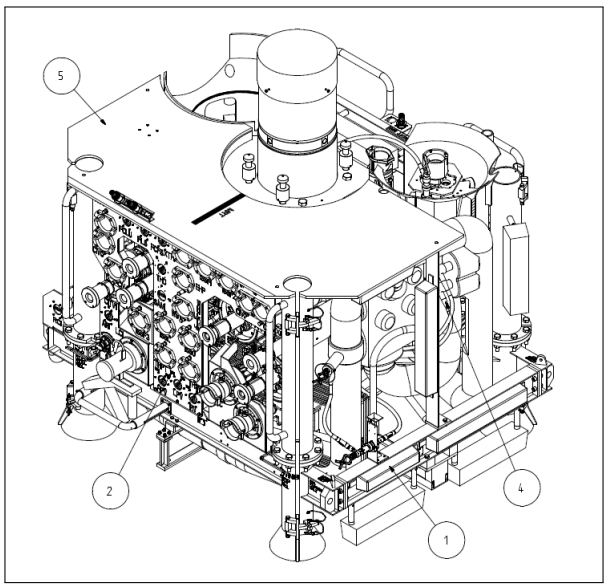

Figure 1.0.2: *A modern XT used in the subsea environment.*

Some physical properties of the XT on figure 1.0.2 are given in table 1.0.1.

Table 1.0.1: XT's physical properties

Property	**Value**
Length	3600 mm
Width	2586 mm
Height	2808 mm
Weight	36000 kg

For the XT to begin its work it needs to be delivered to the seabed. It is vital to ensure the XT's safety during that process. The most risky part of the delivery process is when the tree goes through the splash-zone of the sea. Incoming waves can cause the tree to move, which can in turn cause a crash.

Currently there are no strict criteria determining when it is possible to go through with the delivery process, so the weather conditions are chosen conservatively to ensure safety. This is clearly not optimal and can lead to unneeded prolongation of the time it takes to set up all the hydrocarbon extraction facilities.

Simulating the process of the XT's delivery with the methods of computational fluid dynamics could help determine a less ambiguous criteria to use in practice. This thesis work consists of two parts which are in principal independent yet directed towards the common goal of being able to conduct meaningful simulations of a submergence of a XT.

The thesis was performed in collaboration with the consultant company XDIN AB and using the companies computational resources. The ordering customer of the work was the company FMC Technologies, Kongsberg Subsea.

When modelling complicated phenomena, one is always faced with the need to sacrifice some details of the real-life problem in order to end up with a simulation that is computationally affordable. It is important to sacrifice those details that do not have a qualitative impact on the results.

One of the most important factors affecting the computational cost of any simulation involving a XT is the tree's complicated geometry. Creating an adequate simplified model could thus serve as great assistance to further modelling. The first part of this work is a contribution to the development of such a model.

Previously, Kjemperud [1] constructed a set of three very simplified physical models of the XT and performed several experiments on them in a water basin. The level of adequacy of those models is still to be evaluated, and the obtained drag coefficients should be compared to those of a real tree in the future — an effort to calculate the latter is a current project curated by FMC Technoloies.

Here, a CFD simulation which would reproduce a part of the experiments from [1] is conducted. The reason why this reproduction is required is that some of the results obtained in [1] were surprising, yet no explanation to them was given. By looking at the results of a similar computer simulation one can hope to either find that explanation in the details of the flow pattern or, perhaps, strong evidence that the results were erroneous.

The second part of this thesis directly approaches the task to model the XT's behaviour in the splash-zone. Here the focus is made on taking into account all the physical phenomena present in the splash-zone and a very crude two-dimensional geometrical model is used for the XT.

In the future the two lines of work present in this thesis, if they are further developed, should result in the possibility to conduct simulations with both accurate physics and well-simulated geometry.

2 Evaluating the Drag Force on an XT Model

2.1 Background, Outline and Goals

In [1] the author constructed three simplified scaled models of the Christmas tree. Several experiments were performed in order to determine the hydrodynamic parameters of the models such as the drag coefficient C_D. The acquired measurements are claimed to be scalable since the constructed models are valid as Froude models. To what extent the parameters obtained for the simplified models represent the ones of a real XT is yet unknown.

It is common practice to use experimental techniques and computer simulations in tandem in order to check the accuracy of the results. The goal of the first part of this thesis is to reproduce one of the experiments conducted in [1] as CFD simulations and to give a comparative analysis of the obtained results.

All the details about how the original experiment was conducted can be found in [1], the purpose of it was to estimate the drag forces acting on the model.

We give a rough outline of the setup of the CFD counterpart before discussing each aspect of the simulations in detail. The CADed model of the XT is situated inside a rectangular computational domain which represents a part of the water basin used in [1]. Through one side of the domain the water is considered to flow in at constant velocity. Four different velocities are considered: 0.1, 0.2, 0.3 and 0.4 m/s. By solving the equations of the flow the forces on the walls of the XT model are obtained.

The ANSYS Fluent software package is used to conduct these simulations, as well as for all the other fluid dynamics simulations in this thesis.

2.2 The XT Model

Out the three model proposed in [1] the model referred to as "Model B" is considered here. It consists of three vertical cylinders placed between two horizontal plates and one additional vertical plate on the side. A sketch of the model's geometry is shown on figure 2.2.1. The length of the model is 300 mm. Proper drawings, specifying all the other dimensions can be found in the appendix.

The other models were not considered due to the limited time-span available for conducting this work.

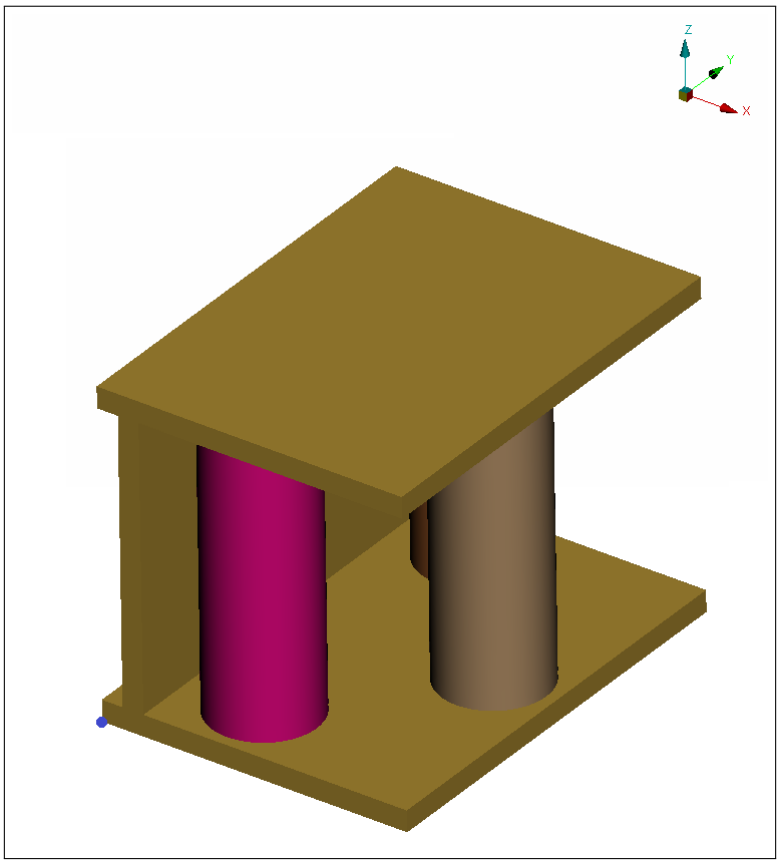

Figure 2.2.1: *Sketch of the model's geometry.*

The coordinate system is chosen to be the same as in [1] for further convenience during results comparison. The origin lies in the lower left corner of the bottom plate seen on figure 2.2.1 (marked with a blue circle) and the axis directions can be seen in the upper right corner of the same figure: Oz points upwards parallel to the cylinders and the vertical plate, Ox points right along the width of the model and Oy points away parallel to the length of the model.

The geometry of the model dictates that the most interesting flow direction for calculating the drag forces is along Oy since it exposes the internal structure of the model. Only this direction will be considered here, while [1] also presents results for Ox and Oz.

2.3 The Computational Domain

The size of the computational domain should be large enough to represent the real water basin used in [1], yet small enough for the simulation to be computationally affordable given a reasonably refined computational mesh.

A rectangular domain of the following size was chosen:

$$\begin{aligned} L_x &= 1020\,\text{cm}, \\ L_y &= 2400\,\text{cm}, \\ L_z &= 1200\,\text{cm}. \end{aligned} \tag{2.3.1}$$

The position of the model in the domain can be seen on figure 2.3.1. Let L_m be the characteristic length of the model along the appropriate direction. Then the position of the model inside the domain is such that along Ox the domain boundaries are $2L_m$ away from the model, along Oy the inlet is $2L_m$ away from the model and the outlet is $5L_m$ away. The treatment of the Oz direction was somewhat different because L_z in (2.3.1) is set equal to the depth of the water tank used in [1] rather then picked out of computational considerations. The same applies to the model's position along Oz, it is placed 0.4 m away from the top boundary of the domain.

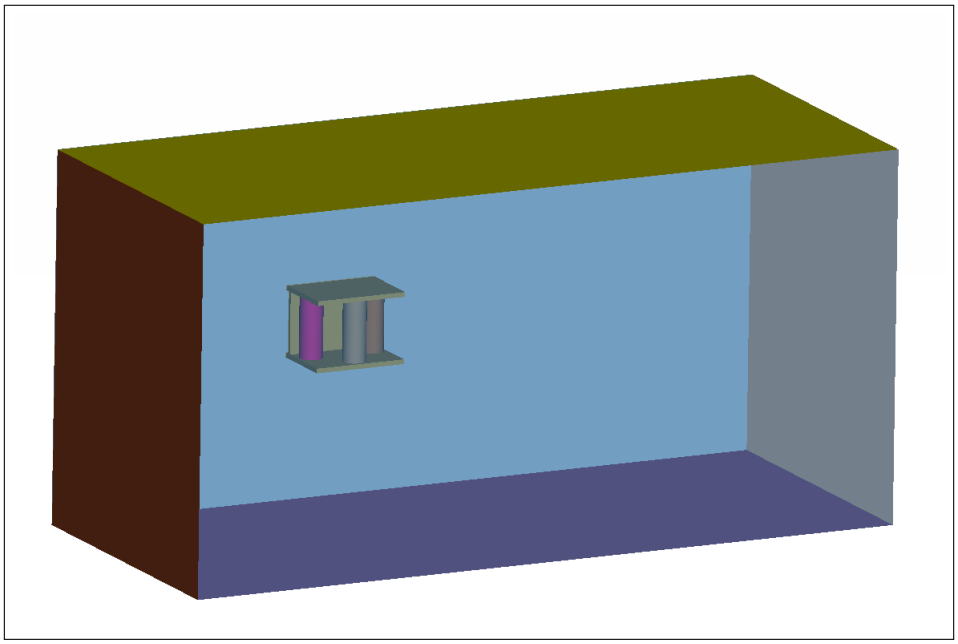

Figure 2.3.1: *Model's position in the domain.*

2.3.1 Boundary conditions

The boundary conditions are summed up in table 2.3.1.

Table 2.3.1: Boundary conditions

Boundary	**Condition**
Walls of the model	Wall with no-slip condition
Bottom wall of the domain	Wall with no-slip condition
Top wall of the domain	Wall with slip condition, $\tau_{ij} = 0$
Side walls of the domain parallel to yOz	Symmetry
Wall behind the model parallel to xOz	Pressure outlet
Wall in front of the model parallel to xOz	Velocity inlet

The symmetry conditions on the side walls reflect the fact that the width of the water tank is several time

larger then the width of the computational domain.

The slip condition on the top wall is set in order to avoid boundary layer formation. The boundary layer is not formed near the surface above the model since in reality it is the free surface of the water. We are however not interested in tracking the position of the free surface because the model is located deep inside the water and the variation in the position of the interface between water and air is therefore negligible. This allows to avoid modeling a multiphase system and greatly reduces the complexity of the problem.

2.3.2 Initial Conditions

In order to obtain a good initial guess of the solution a technique called Hybrid Initialization in ANSYS Fluent is used.

In order to obtain the velocity field a Laplace equation is solved for the velocity potential ϕ with boundary conditions concordant with those prescribed for the velocity field. The velocity field is then prescribed as $\nabla\phi$.

Pressure and the turbulent parameters are initialized as constant, based on the boundary condition at the inlet.

2.4 The Computational Mesh

Since the geometry of the model and the domain is fairly simple, it is possible to construct a structural hexahedral mesh.

The computational power available allowed for maximum 10 million cells.

The pre-processing software ANSA was used build the mesh.

2.4.1 The Surface Mesh on the Model

The surface mesh on the model's walls should be quadrilateral in order to later produce a hexahedra volume mesh later. Also the size of the surface mesh will directly affect the size of all the volume cells in the domain, since the later will be produced by mapping the surface mesh. Figures 2.4.1, 2.4.2, 2.4.3 display various parts of the surface mesh. Special focus is given to the parts were the mesh has to be fine enough to resolve boundary layers.

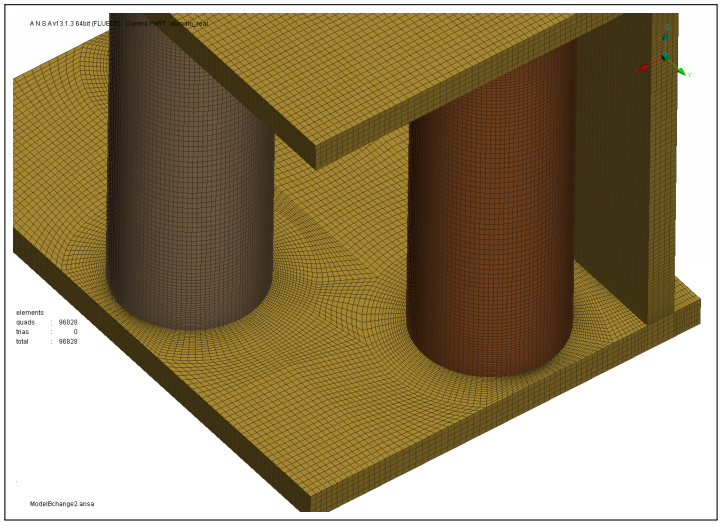

Figure 2.4.1: *Overview of the surface mesh on the model.*

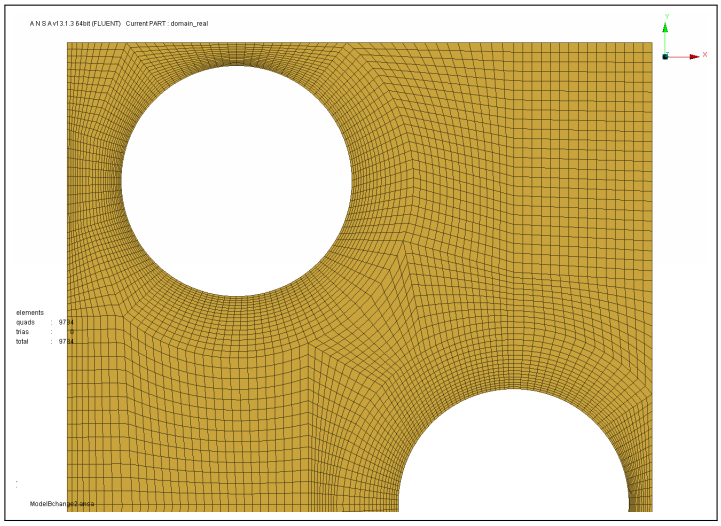

Figure 2.4.2: *Surface mesh on a part of the inner surface of the horizontal plates.*

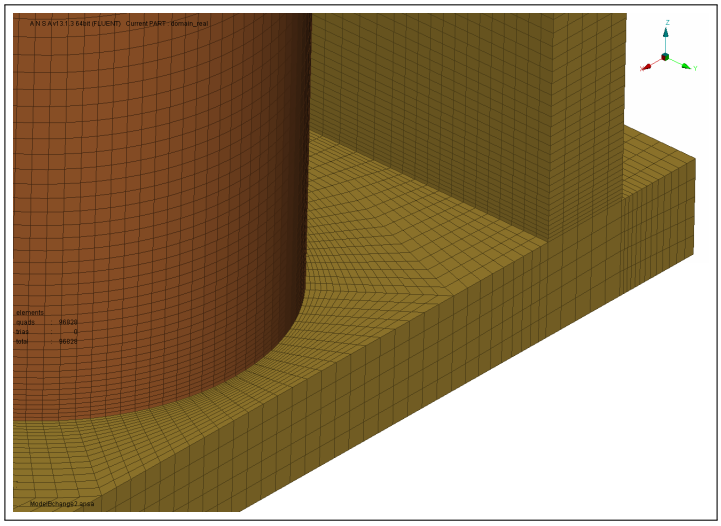

Figure 2.4.3: *Surface mesh for resolving the boundary layers of the cylinders and the vertical plate.*

A total number of 96828 quadrilaterals constitutes the mesh. A rough estimate of the length of a cell's side is 3.5 mm.

2.4.2 The Volume Mesh

Inside the Model

The construction of the volume mesh begins with meshing the space inside the model. The meshing was done by directly mapping the surface mesh of the inner surface of the bottom horizontal plate to the corresponding surface on the upper plate. The resulting volume mesh is shown on figure 2.4.4. It consists of 1096700 hexahedra.

Outside the Model

The rest of the domain was meshed by first mapping the faces forming the outer surfaces of the model to the boundaries of the domain, see figure 2.4.5. The growth factor applied along the the mapping is 1.1. The maximum length of a cell is about 139 mm.

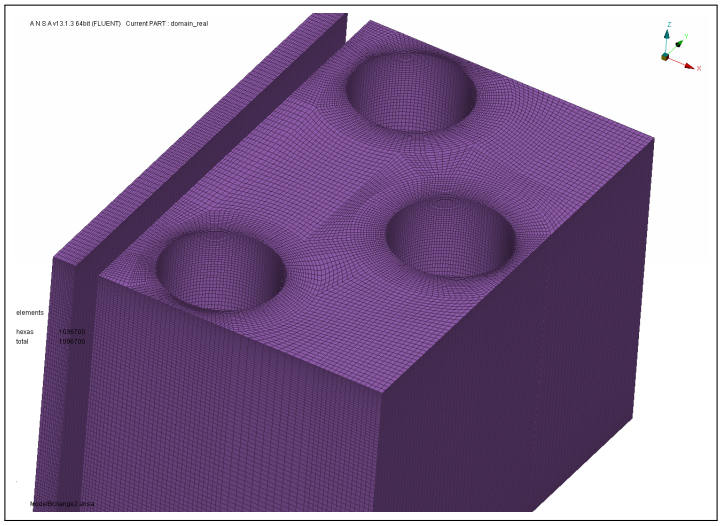

Figure 2.4.4: *The volume mesh inside the model.*

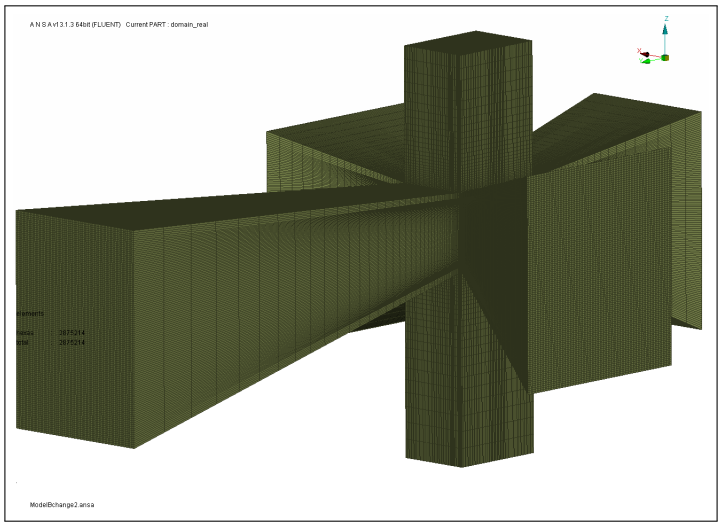

Figure 2.4.5: *First stage in meshing the domain around outside the model.*

The rest of the mesh is done by mapping the sectors that are left. They are indirectly visualized on figure 2.4.6 which shows the additional help surfaces constructed to assist the mappings.

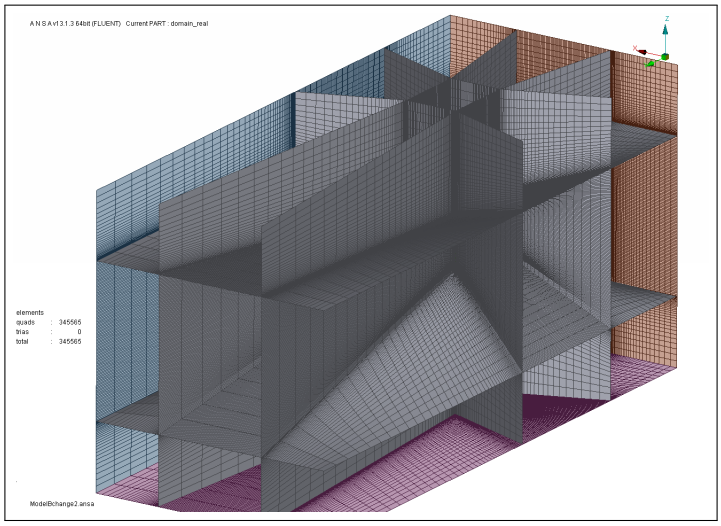

Figure 2.4.6: *Help surfaces (grey) for mapping the volume mesh outside the model.*

The completed volume mesh is shown in figure 2.4.7. The total number of cells is 4502342 which is affordable computationally and moreover leaves space for refinement.

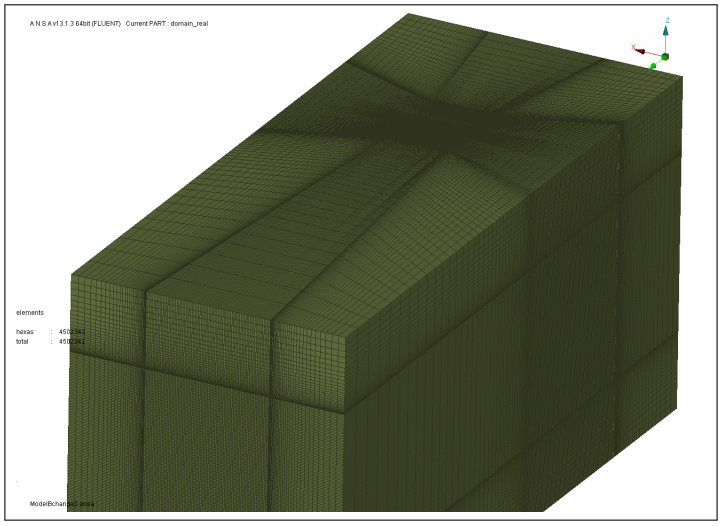

Figure 2.4.7: *The complete volume mesh, overview.*

2.5 Modelling the Fluid Flow

Here we discuss the various possibilities for modeling the fluid flow using ANSYS Fluent and then make a choice of models and methods best fit for the current simulation.

2.5.1 Turbulence Modeling

In order to correctly model the flow we have to evaluate its Reynolds number. For a characteristic length we take the XT model's size along the Oy direction. For a characteristic speed we choose the minimal inlet velocity, which is 0.1 m/s. This gives

$$Re = \frac{\rho u l}{\mu} = 33708. \tag{2.5.1}$$

We can conclude that we are dealing with the turbulent flow.

Currently there is no unified approach towards turbulence modeling. Due to computational efficiency the so called eddy viscosity models are the most wide-spread when it comes to engineering applications. It is

assumed that all the flow variables can be divided into a time-averaged and a fluctuating part. Thus, say, for velocity U one can write $U = \bar{U} + u$, where $\bar{U}$ is independent of time for a steady problem. By substituting the flow variables in the Navier-Stokes equations with such decompositions one arrives to the Reynolds-averaged Navier-Stokes equations, commonly abbreviated as RANS:

$$\frac{\partial \rho \bar{U}_i}{\partial t} + \left(\rho \bar{U}_i \bar{U}_j\right)_{,j} = -\bar{P}_{,i} + \left[\mu\left(\bar{U}_{i,j} + \bar{U}_{j,i}\right) - \rho\overline{u_i u_j}\right]_{,j}, \tag{2.5.2}$$

where $(\cdot)_{,j}$ stands for differentiation with respect to x_j.

The new unknown term $\overline{u_i u_j}$ in (2.5.2), called the Reynolds stress tensor, demands introduction of additional equations in order to achieve closure. Eddy viscosity models use a relation called the Boussinesq assumption to connect the Reynolds stresses to velocity gradients:

$$\rho\overline{u_i u_j} = -\mu_t\left(\bar{U}_{i,j} + \bar{U}_{j,i}\right), \tag{2.5.3}$$

where μ_t is the eddy or turbulent viscosity which is unknown. Models vary in their approach for determining μ_t.

There are several of eddy viscosity turbulence models developed, ANSYS Fluent lets the user choose among eight. Additionally one can apply certain modifications to each model to tune it for better performance in certain cases. Even though some models are generally more accurate then the other, each of them is known to behave well for certain types of flow and worse for other.

Often the so called two-equation models are used due to their wide applicability. In such models, transport equations for two scalar quantities are added to the system. Most terms in these exact equations are then substituted by simpler expressions which still represent the same physical processes. The equations obtained after these substitutions are called the modeled equations. Eddy viscosity is calculated through a relation with the added two scalars, this relation is derived on dimensional grounds.

The most commonly used two-equation model is the $k-\varepsilon$ model, where modelled equations for turbulent kinetic energy k and turbulent dissipation ε are added. After the model has been extensively used, modified $k-\varepsilon$ models were introduced which were intended to address the original model's weaknesses.

The $k-\varepsilon$ Realizable model modifies the ε equation and the way eddy-viscosity is calculated to insure that the normal Reynolds stresses always stay positive or "realizable" in the sense that they satisfy a certain physical constraint. The $k-\varepsilon$ Realizable model was substantially validated for various types of flows and was found to almost always outperform the original $k-\varepsilon$.

The standard $k-\omega$ model incorporates an equation for turbulence frequency $\omega = \varepsilon/k$ instead of ε. This allows for integrating the equations all the way to the wall. The downside of the model is that it is sensitive to the free-stream parameters of the flow.

The Shear Stress Transport (SST) $k-\omega$ model was developed to effectively blend the $k-\varepsilon$ and $k-\omega$ models to benefit from the pluses of both [3]. The standard $k-\omega$'s and modified $k-\varepsilon$'s equations are both multiplied by a blending function and added together. The blending function is designed in a way that near the wall the $k-\omega$ model is used while the $k-\varepsilon$ is used elsewhere.

2.5.2 Solver Algorithm

All the numerical algorithms for solving the flow equations in Fluent can be divided into two groups: the pressure based and the density based. Although in the later versions of Fluent all algorithms are applicable for a broad range of flow problems, the density based ones were historically designed to deal with high-speed compressible flows and the pressure based were targeted towards incompressible low-speed problems. Since the task at hand falls into the latter class, it can be beneficial to stick to the pressure-based algorithms.

There are two types of pressure based algorithms available in Fluent: segregated and coupled. Segregated algorithms solve all the flow equations separately. The SIMPLE algorithm is an illustrative example: first the three momentum equations are solved sequentially for a guessed initial pressure field, then a correction for the pressure field is obtained from the continuity equation, this correction is used to update the velocities and the next iterations starts. This is then repeated until convergence, i.e. until the pressure correction is near zero.

In contrast with the above the coupled algorithm solves the momentum equations and the continuity equation simultaneously.

The segregated algorithms are somewhat better suited for transient problems, since each iteration is less computationally expensive. For steady problems the coupled algorithm is usually preferable since, in spite of the larger time cost of a single iteration, the decrease in the amount of iterations required for achieving convergence makes the total time less.

2.5.3 Discretization

In order to obtain algebraic equations instead of differential Fluent uses the finite volume method. The values of the scalar variables are stored in the center of the cells.

After the equations are integrated over a control volume a proper discretization scheme has to be applied to approximate the convective fluxes through the cell boundaries and the spacial derivative in the diffusion terms.

The latter is readily approximated with the central difference scheme, which has second order accuracy and is stable.

The first order upwind scheme assumes that at the cell boundary the scalar variables are equal to their respective values in the center of the upwind cell.

Higher order of accuracy is desirable especially for discretizing the momentum equation. The second order upwind scheme calculates the variable's value at the cell face ϕ_f as a sum of its value at the center of the upwind cell ϕ plus the value gradient of that variable at the center of the upwind cell $\nabla\phi$ times the distance between the upwind cell's center and the face d:

$$\phi_f = \phi + d\nabla\phi.$$

Using discretization schemes of even higher orders would give additional convergence problems, but not necessarily increase the accuracy of the solution because the modeling error introduced by using RANS turbulence models would be greater then the error of the discretization.

2.5.4 Solution Strategy

The following strategy was applied to get an accurate result. First the $k-\varepsilon$ Realizable model with the first order upwind discretization scheme for all equations was used to obtain a good starting approximation of the solution. This was needed to help converge the $k-\omega$ SST model, which was applied afterwards along with the second order upwind scheme for the momentum equations.

The amount of iterations spent with the $k-\varepsilon$ model was not strictly determined, full convergence was not necessarily achieved with it. Rather the switch to $k-\omega$ SST was made when the solutions seemed to be settled on a direct path towards convergence with no high oscillations occurring from iteration to iteration. Sometimes the available time frame also played a significant role.

2.6 Results

Table 2.6.1 shows the value of different components of the forces on the XT model obtained with CFD modeling and in [1].

Table 2.6.1: Forces on the XT model. Results from CFD modeling and experimental results from [1].

Speed at inlet, [m/s]	**Force component**	**Value, CFD, [N]**	**Value, experiment, [N]**
0.1	F_x	-0.12	-0.22
	F_y	0.19	0.117
	F_z	0.00	0.25
0.2	F_x	-0.47	-1.01
	F_y	0.73	0.59
	F_z	-0.00	-0.59
0.3	F_x	-0.78	-2.52
	F_y	1.96	1.39
	F_z	-0.00	-0.10
0.4	F_x	-1.63	-3.64
	F_y	2.86	2.28
	F_z	-0.00	0.37

Let us focus on the results of the CFD modeling before making the comparison with the results from [1].

The z component of the force can be considered to be zero since the deviations from zero are negligible for all four values of the speed at the inlet. That is reasonable since the design of the model contains no parts that would cause the flow to redirect towards the two horizontal plates.

The y component of the force is predictably the highest in magnitude and increases along with the increase of the speed at the inlet.

The magnitude of the x component of the force is quite high, despite the x direction being perpendicular to the direction of the flow at the inlet. Figure 2.6.1 shows the pressure distribution inside the model in the plane between the two horizontal plates. It is visible that the pressure to the right of the vertical plate is generally higher then to the left of it, resulting in the registered force in the $-x$ direction. The pressure is increased in front of the cylinders which is typical behaviour for a flow around an obstacle. Additionally the small distance between the vertical plate and the two left cylinders make the increase in pressure spread closer towards the wall.

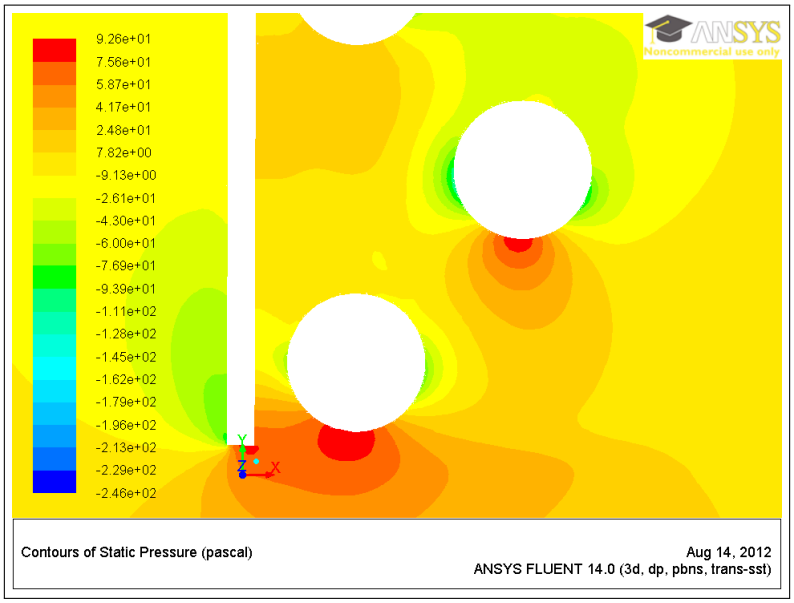

Figure 2.6.1: *Static pressure distribution inside the XT model, $u_{inlet} = 0,4$ m/s. Cut at $z = 115$ mm, parallel to xOy.*

Comparing, we observe significant difference between the experimental and CFD modeling results. The former show high force components in directions perpendicular to the flow direction, which is hard to explain physically. The results provided by the CFD simulation are more realistic and the distribution of force magnitude between the different directions is more concordant with what one expects intuitively.

Such extra forces in the x and z directions could appear if the XT's model was perhaps not properly fastened during the experiment and given a small rotational degree of freedom. It is hard to conclude how these errors affected all the other results in [1], but it is obvious that they need verification as soon as the origin of the errors in the experiment modeled here is eliminated.

However the CFD results are likely to also be relatively far from exact due to using RANS for modeling turbulence. Even though these models work well for predicting the flow pattern, if a very accurate quantitative result is required different models like large eddy simulation or direct numerical simulation should be used.

In spite of that, the value of the obtained results lies beyond just showing that the former experimental results were probably highly erroneous. Their accuracy is sufficient for comparison with new experiments if those are to be conducted. They can be used as a guide line for developing more complicated models, which is most likely needed, since all the models in [1] are very simplistic.

3 Simulating the XT's Behaviour in the Splash-Zone

3.1 Outine and Goals

Reproducing the behaviour of the XT in the splash-zone is a complicated task due to the multiple amount of complex physical phenomena driving it.

Since the XT is hanging in the air supported by the riser with the sea below it, the fluid flow problem is multiphase. A realistic way to model sea waves has to be found. Also, it is unknown whether the waves hit the XT with enough force to cause its significant movement. In order to check that, FSI (fluid-structure interaction) has to be considered, thus adding a structural mechanics component to the problem. The real geometry of the XT is also very complex.

In order to make the experiment computationally affordable it is necessary to adopt some simplifications. We found it to be most reasonable to completely sacrifice the geometrical complexity of the problem, while leaving all the physical content intact. The consequence of this approach is that quantitatively the obtained results would not be reliable. However the results would be meaningful qualitatively. Developing the methodology of setting up this kind of problem in the ANSYS software package is also valuable on its own. Given the methodology conducting similar experiments with more complex geometry later is merely a matter of additional computational power and time invested into CADing and meshing.

Ignoring the true geometry of the XT also allows to consider the problem in just two dimensions. The XT is then represented as a rectangle with length, width and mass set according to its the real dimensions. The computational domain is also rectangular with the waves generated on the left boundary, while the right and top boundary serve as outlets.

To conclude whether it is necessary to take into account FSI, two experiments would be performed. In the first experiment the XT would be considered static, with wall boundary conditions imposed on its sides. In the second the XT would be connected to a pipe, approximately 30 long. The other end of the pipe would be fixed.

During the time frame of the experiment two waves would hit the XT. The x and y components of the force acting on the XT would be continuously monitored.

3.2 The XT Model

The XT is modeled by a rectangle of length 3600 mm and height 2808 mm. Due to requirements of the ANSYS software package in order to include FSI in the model the geometry should be three-dimensional. Therefore a certain thickness was also added to the rectangle.

The riser is geometrically represented by a line body connected to the center of the top surface of the XT and to a point on the top surface of the computational domain exactly above the XT. In order to define the physical properties of the line body it is given a cross-section. Since the riser is a pipe in its form, a pipe cross-section is defined with an outer diameter of 219.1 mm and inner diameter of 177.8 mm.

3.3 The Computational Domain

3.3.1 Suitability for Wave Modeling

The domain has to be large enough for the waves to have time to form as they emerge from the left boundary. Also significant space should be left to the right of the XT so that the waves would have time to die out. After testing with various sizes the domain length was set to 25 m, with the XT placed in the middle. This size is large enough to simulate two-three waves hitting the XT, but a larger domain is needed to run longer simulations. Ideally the XT should be placed two-three wavelengths away from the left boundary, so that the chaotic flow near the XT that arises after the hit of the first wave does not affect the formation of the waves.

3.3.2 Blockage Problem

Since the water from the waves was not expected to reach areas high above the XT, the upper boundary of the computational domain was originally placed about two meters above the XT. This resulted in completely unrealistic behaviour of the fluids. The water below the XT would accelerate to very high velocities and rush towards the outlet boundary on the right.

The roots of the non-physical behaviour lied in the artificial reduction of the dimensionality of the problem. As illustrated on figure 3.3.1 the air enters the domain through the left boundary with some initial speed v_0. Since a big part of the domain is blocked by the XT, mass conservation dictates that the velocity of the air will increase, especially in the small gap between the XT and the water. This strong wind makes the water behave unrealistic as well. In reality the effect is negligible because the air would flow around the XT from all sides and the XT is not entirely impenetrable for air.

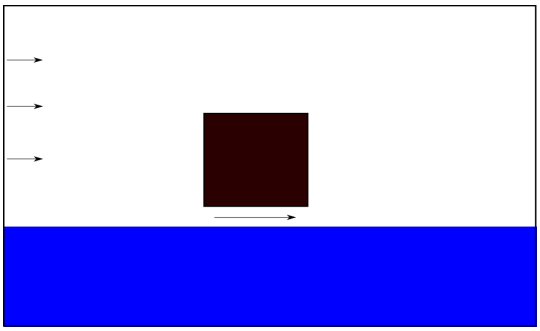

Figure 3.3.1: *Schematic illustration of the blockage problem.*

In order to avoid the blockage problem the hight of the domain was significantly increased and set to 39 m.

The computational domain is shown on figure 3.3.2.

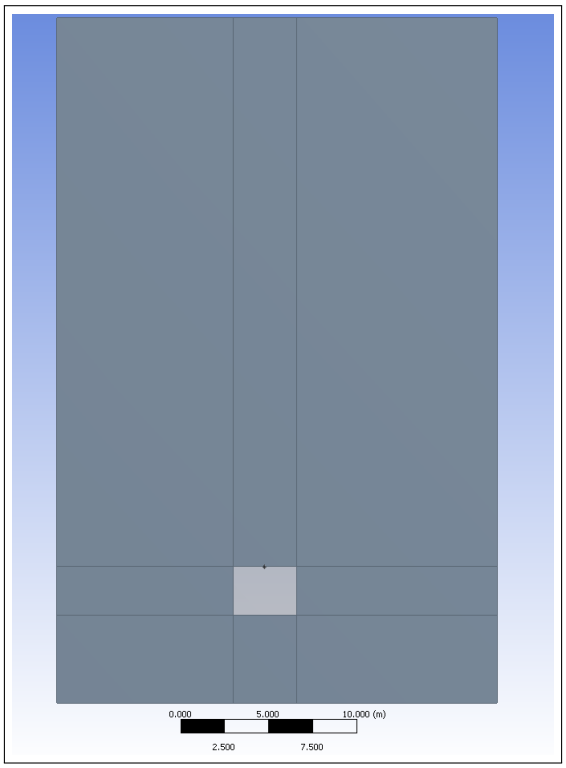

Figure 3.3.2: *The computational domain.*

3.4 The Computational Mesh

3.4.1 Mesh for the Fluid

The simple geometry makes the fluid domain easy to mesh with a hexahedra mesh. ANSYS Meshing was used to create the mesh.

Figure 3.4.1 shows the mesh between the left boundary of the domain and the XT. The mesh is made finer near the boundaries.

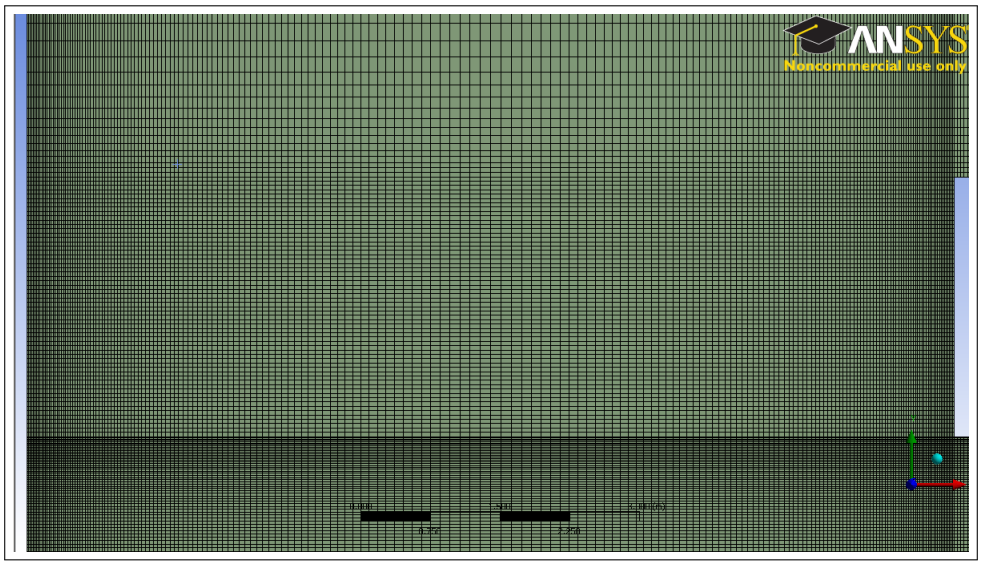

Figure 3.4.1: *Mesh between the XT and the left boundary.*

The length of the cells increases significantly further above the XT. The length of the longest cell, adjacent to the top boundary is approximately 2.5 m. That is done to decrease the computational costs. We allow the mesh to be so coarse in the upper part of the domain because the characteristics of the flow there are of no interest — the whole upper area is dedicated purely to solving the blockage problem.

The depth of the mesh was set equal to the depth of the domain in order to keep the problem effectively two-dimensional.

3.4.2 Mesh for the XT

When modelling FSI the XT has to be meshed as well. ANSYS Mechanical uses the finite element method for discretization, therefore the mesh consists of elements of a certain type.

Since the contact between the XT and the line body is located in the middle of the XT's top wall, the mesh has to be at least two elements thick.

The XT is meshed with TET10 elements, which refers to tetrahedra with 10 nodes: one in the middle of each side and one in each vertex. The mesh is shown on figure 3.4.2.

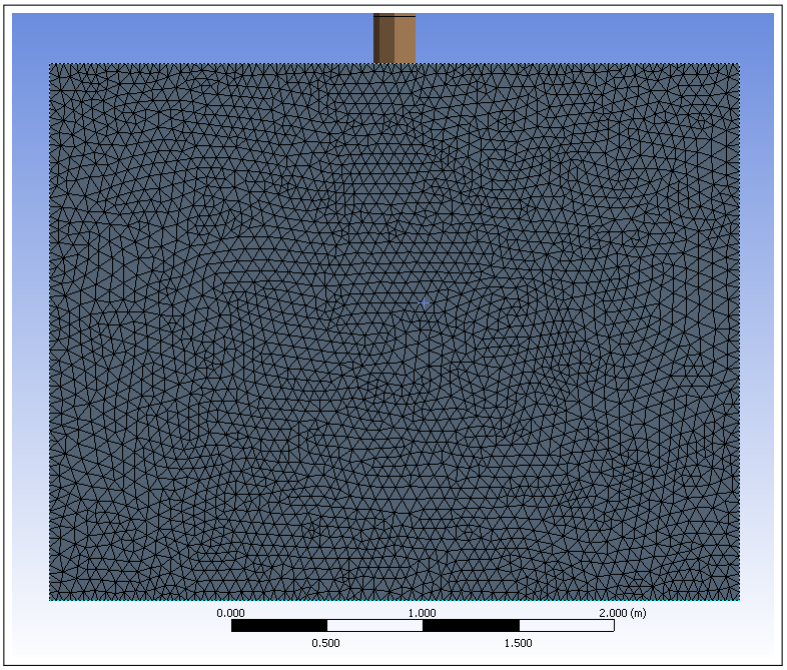

Figure 3.4.2: *The mesh of the XT.*

The line body is meshed with PIPE16 elements (figure 3.4.3) , which are designated for modeling deformation of elastic pipes.

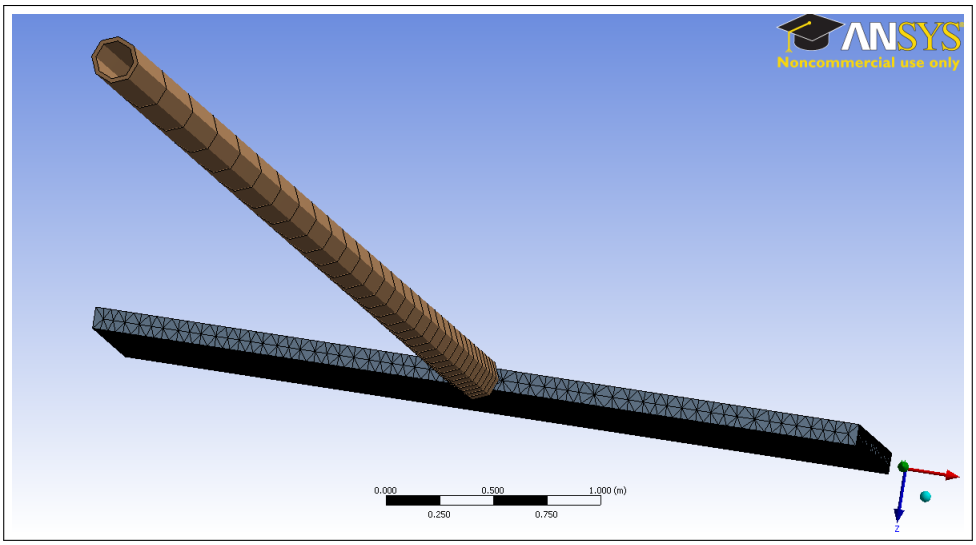

Figure 3.4.3: *The pipe elements on the linear body.*

3.5 Boundary Conditions

The boundary conditions are summed up in table 3.5.1.

Table 3.5.1: Boundary conditions

Boundary	**Condition**
Walls of the XT	Wall with no-slip condition or Fluid-Structure Interface
Bottom surface of the domain	Wall with no-slip condition
Top surface of the domain	Pressure Outlet
Side surfaces of the domain parallel to xOy	Symmetry
Left surface of the domain	Wave generation
Right surface of the domain	Pressure outlet

The boundary condition on the XT is set to be a wall in case of the simulation with a static XT. In the simulation with FSI the walls of the XT are set to a special boundary condition called the Fluid-Structure Interface in ANSYS Mechanical. This boundary condition points out the surfaces over which data transfer between the structural and fluid dynamics solvers will occur. The way FSI is organized in the ANSYS software package will be discussed in detail below.

The top surface is set as outlet thus letting air freely exit the domain through the top. This is done to further fight the blockage problem discussed above.

The boundary condition on the left surface is set to a special condition built into ANSYS Fluent called "wavy". This condition allows for wave generation. This topic deserves special attention and is covered in detail in section 3.6.1 below.

The pressure outlet on the right allows the waves to get out of the domain. The condition on the bottom surface does not play a significant role in the simulation, since all the active processes are in a good distance away from it, both wall and symmetry would be suitable. The side surfaces are in the simulation only because ANSYS enforces a three-dimensional domain. The symmetry condition imposed on them insures that they don't introduce additional restrictions on the flow variables.

3.6 Modeling the Fluid Flow

3.6.1 Generating Waves

A method to generate waves at the left boundary of the domain had to be found. The required method should be such that it is easy to control the characteristics of the waves.

It was already mentioned above that a special boundary condition embedded into Fluent was used to generate the waves, however two other methods that proved to be less successful in practice are mentioned first.

Pre-patching a Water Column

One attempt was to pre-patch a column of water near the left side of the domain. Immediately after the beginning of the computations the "breaking dam" effect would occur, i.e. the column would collapse. The expectation was that the collapse would result in a wave or several waves propagating along the domain.

Despite the collapse of the column causing a large perturbation and as consequence a wave, the characteristics of that wave were very hard to control. Moreover, since the experiment requires a series of waves with similar characteristics, the approach was given up.

Using a Dynamic Mesh

In [4] the authors describe a method for generating waves by using a dynamic mesh. The idea behind this method is that if the left boundary would harmonically move back and forth it would act as a piston. The resulting water motion would result in a wavy surface.

This method works well, at least for generating waves with low steepness. The downside is that the dynamic mesh introduces extra complexity.

Using Fluent's Built-in Wave Generator

Ansys Fluent has a special built-in boundary condition for generating waves, called "wavy". In order to generate waves the user has to pick the boundary at which the waves would be generated and choose the values of several parameters, the most important of which are:

Wave theory There is a number of wave theories that Fluent can base the wave generation on. A discussion of the available theories and their suitability is given below.

One also has to choose whether the deepness of the water can be considered infinite or not. In the case of this simulation the height of the free surface is only several meters away from the bottom, so shallowness has be considered in the wave modelling.

Wave amplitude Was set to 1.2 m to simulate relatively violent waves yet those that might still be considered suitable for going through with the XT's delivery.

Wave length Was set to 30 m to decrease the steepness of the waves. Relatively low steepness is needed to stay below the waves' braking limit.

Free surface level The height at which the free surface is located. Considering the amplitude of the waves and the size of the computational domain a height of 5 m was chosen.

The choice of wave theory lies between linear Airy waves and higher order non-linear Stokes waves, which can go as high as fifth order. The order refers to the number of harmonics used to represent the waves' profile. The linear theory gives a simple harmonic wave, while the Stokes waves are modelled with adding higher order harmonics.

There are several criteria which the chosen waves parameters have to fulfil. The criteria are different for linear and non-linear waves and can therefore determine the choice of the wave theory. The criteria in case of shallow water waves are:

- Wave height H to liquid depth h ratio: $\left(\frac{H}{h}\right)_{max} = 0.78$.
- The wave height to wave length ratio: $\left(\frac{H}{\lambda}\right)_{max} = 0.142 \tanh\left(2\pi\frac{h}{\lambda}\right)$ for linear waves, $\left(\frac{H}{\lambda}\right)_{max} = 0.0625 \tanh\left(2\pi\frac{h}{\lambda}\right)$ for non-linear waves.
- The Ursell number, defined as $\mathrm{Ur} = \frac{H\lambda^2}{h^3}$: $\mathrm{Ur} < \frac{32\pi^2}{3}$ for linear waves and $\mathrm{Ur} < \frac{8\pi^2}{3}$ for non-linear waves.

The second criterion is weaker for non-linear waves, allowing smaller wave lengths for a given wave height. That is desirable because it allows to decrease the waves' period and thus simulation time. Thus the linear theory was disregarded.

Experimenting with different non-linear theories, we found none of them to perform exceptionally better then the other. According to [8] second and fourth order wave theories are prone to produce secondary crests. With that in mind the third order Stokes theory was chosen.

3.6.2 Turbulence Modeling

Given the typical velocities of 3-5 m/s the water flow is clearly turbulent. However accounting for turbulence would not change the results of the simulation qualitatively. It is the interaction between the waves and the XT that is central, not the peculiarities of flow pattern of the water and air. Given the form of the waves and their general properties, which are regulated by the boundary condition, the impact the waves cause would stay nearly the same independent of the presence of a turbulence model.

Getting an exact number (i.e. as exact values of the forces on the XT's walls as possible) was not the goal of the simulation a priori. This is a direct opposite to the matters in the simulation described in the first part of this thesis. There the goal indeed was to resolve the fluid flow as accurate as possible in order get a correct value of a certain quantity, therefore turbulence modeling was a major concern.

In conclusion the decision to model the flow as laminar was made in order speed up the computation.

3.6.3 Solver Algorithm

The multiphase flow model which used in the simulation (discussed below) is only available in conjunction with the pressure based solver in Fluent.

As discussed above it is more reasonable to use a segregated pressure-velocity coupling algorithm when dealing with transient flow. However care has to be taken to verify that the amount of iterations the solver is allowed to do per time-step is large enough to get convergence.

By monitoring the area weighted average of the pressure on the XT we observed that 20 iterations of the SIMPLE algorithm are sufficient for convergence.

3.6.4 Multiphase Flow Modeling

There are two phases present in the simulation: air and water. The flow can be classified as stratified. In fact we are not interested in the air flow at all, the goal is to model the free surface of the water and keep good track of the interface between the phases.

The Volume of Fluid model allows to track the interface accurately enough for the scales our simulation operates in and performs best for stratified flows. Other models are more focused on the situation when one phase is dispersed within another. Another argument for choosing this model is that it uses a single set of momentum equations to calculate the flow of both phases.

The VOF model keeps track of the interface by introducing a color function α for each phase. The color function takes the following values:

0, if the phase is not present in the computational cell;

1, if the phase takes up the whole cell;

$(0; 1)$. if the cell contains more then one phase.

An advection equation is solved for the color function of each phase thereby updating the position of the interface. In case of two-phase flow only one equation needs to be solved, since the value of the color function of the second phase α_2 can be obtained as $1 - \alpha_1$. More generally one "primary" phase is defined and advection equations are solved for all the remaining "secondary" phases. The constraint $\sum_i \alpha_i = 1$ is then used to calculate the value of the primary phase's color function in each cell.

The values of the color functions are used get the values of physical properties like density, viscosity etc. As the color functions represent the volume fractions of the phases in a cell their values are used as weights in the weighted sum used to calculated the physical properties, for instance for density in a two-phase system:

$$\rho = \alpha_2\rho_2 + (1 - \alpha_2)\rho_1.$$

These physical properties are present in the momentum equations therefore the shared velocity field produced by solving it takes into account the difference in the phases.

3.6.5 Discretization

General comments on how Fluent discretizes equations were already given in the previous part of the thesis. Here we focus on the choice of the discretization schemes.

The second order upwind scheme was chosen for the momentum equation for better accuracy.

Choosing the discretization scheme for the color function's advection equation was less trivial. The availability of certain schemes is dependent on whether the discretization of the convective terms in time is explicit or implicit.

The most accurate scheme available in Fluent according to [8] is the geometric reconstruction scheme, which uses a piecewise-linear approach to reconstruct the interface between the phases. However it is only available in coupling with the explicit discretization in time and choosing implicit discretization allows to use larger time-steps without loosing the sharpness of the interface.

After experimenting with different schemes and time-steps we found it best to stick to a time-step of 0.005 sec, which was small enough to use the geo-reconstruction scheme, yet large enough for the simulation to be finished within a timespan of several hours. Using larger time-steps led to poor capturing of the waves-XT interaction.

3.7 Fluid-Structure Interaction

3.7.1 FSI in ANSYS Workbench

Fluid-structure interaction involves coupling together two completely separate physical problems. The mathematical methods used for solving the governing equations of these problems can also be very different from each other. Therefore in practice two separate solvers are usually used: one for fluid dynamics and one for structural. In order to couple the solvers together a method for transferring data between them is required. Additionally the work of the solvers should be synchronized to make sure that one of them does not move on to the next time-step until the other is also ready for it.

The ANSYS software package provides a special tool, called System Coupling which takes care of the synchronization and data transfer between Ansys Fluent and ANSYS Mechanical, the latter being the structural solver.

The global layout of the FSI problem is set up in the ANSYS Workbench, which serves as an umbrella over all the different software ANSYS provides. As seen on figure 3.7.1 the layout consists of four interconnected components:

A Transient Structural — the structural part of the problem is defined here.

B Fluid Flow (FLUENT) — the fluid dynamics part of the problem is defined here.

C Results — this component is used to view the results from both solvers together in ANSYS CFD-Post.

D System Coupling — the service taking care about the coupling between the two solvers.

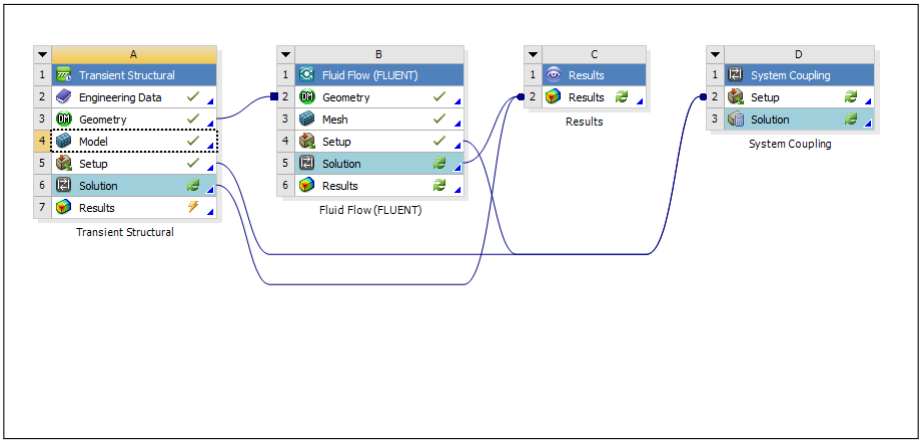

Figure 3.7.1: *The layout for solving an FSI problem in ANSYS Workbench.*

The blue lines show the connections between the components:

- Fluent and Mechanical share the global geometry of the problem, even though each solver is aware only the part of the domain relevant to its task.
- The Setups of components A and B are connected to the Setup of the System Coupling. This is needed for the System Coupling to be aware of which components are being coupled and over which surfaces will the data-transfer occur.
- The Solutions from Fluent and Mechanical are connected to the global Results component.

Without going deep into all the steps needed to create the layout described above we would like to acknowledge here that we found the process to be user-friendly and straight-forward. The general layout is built exclusively by drag-and-droping the required components from a complete list of the components available and selecting the parts of the chosen components one wants to connect.

The only inconvenience we experienced is that coupling the geometry forces one to do the meshing in ANSYS Meshing and, to some extent, do the CADing in ANSYS Design Modeller. If one chooses to import a mesh, then the Workbench is unable to extract the CAD data from it and share it with the other component.

3.7.2 The System Coupling Service

The System Coupling Service is responsible for all communication between the solvers and their synchronisation. Besides for that it initializes and shuts down the solving process when the solvers have reached the appropriate time step set by the user. To communicate with the solvers the Service uses a commercial TCP/IP based protocol.

At each time step the Service drives the solving process through the following steps which comprise a coupling iteration:

1. The order in which the solvers will execute is set.

2. The solvers collect the required data and solve.

3. A convergence check is performed. Convergence is assumed to be achieved if both solvers report that they have converged according to the their internal convergence criteria, and additionally the data transfers have converged.

4. If the solution is converged the solvers proceed to the next time step, otherwise the next coupling iteration starts.

As indicated in step 3 in the list above the Coupling Service monitors convergence of the data transfers. Below we present the characteristics of the transfers that are used for monitoring convergence.

Let ϕ_l be value of the variable transferred from one solver to the other at location l. Let $\Delta_l = \frac{\phi_l^{i+1} - \phi_l^i}{\omega}$ be the change in ϕ_l between two consecutive coupling iterations, where ω is an underrelaxation factor. Then let the normalized change in ϕ_l between consecutive coupling iterations be

$$\hat{\Delta}_l = \frac{\Delta_l}{0.5((\max|\phi_l| - \min|\phi_l|) + |\overline{\phi_l}|)}.$$

Two measures of data transfer convergence are used by the System Coupling Service: the maximum of $\hat{\Delta}_l$ and its RMS $= \sqrt{\overline{\hat{\Delta}_l^2}}$. The averaging is performed over all transfer locations.

3.7.3 Data Transfer Algorithms

There are two data transfer algorithms used by the System Coupling Service: the Profile Preserving algorithm and the Conservative Profile Preserving algorithm. The main difference between them is that the latter is locally conservative. Therefore it is used when the transferred value is conserved (mass, momentum etc.). The other algorithm is used for transferring non-conservative variables (displacement, temperature).

Each algorithm works in three steps.

Mapping The target surface is being matched with the source surface. In other words a correspondence between the "nodes" comprising the source surface and those of the target surface is set up. The definition of a "node" can differ depending on the mapping algorithm but it is always some simple geometrical part of the surface. The correspondence between a particular target node and a source node is measured with a number — a weight.

Interpolation The value of the transferred variable on the target nodes is then calculated as a weighted sum of the values on the source nodes: $\phi^{trg} = \sum_i \omega_i \phi_i^{src}$. The weights here are those obtained by the mapping algorithm.

Under-relaxation In order to improve convergence the value of ϕ is under-relaxed: $\phi_{new} = \phi_{old} + w(\phi_{new} - \phi_{old})$. This is particularly important when large structural deflections occur.

The two algorithms used by the Coupling Service differ only in the mapping algorithm they use. The Profile Preserving algorithm uses the Bucket Surface mapping algorithm presented in [5], while the Conservative Profile Preserving algorithms uses the General Grid Interface mapping algorithm [6].

3.7.4 Dynamic Meshing

When the XT is displaced Fluent needs to update the computational mesh. There are four methods for dynamically updating the mesh in Fluent.

Re-meshing The cells around the moving boundary are locally re-meshed. The method is good when displacements are big and other methods therefore fail. This method is only available for tetrahedral meshes.

Layering New layers of cells adjacent to the boundary are added as the boundary moves. This method is good for sliding boundaries, when little rotational movement is present. The method is only available for prismatic meshes.

Spring-based Smoothing The edges between the nodes of the mesh are assumed to be ideal strings. The state in which the strings are at before the boundary moves is considered to be equilibrium. The displacement of the boundary acts as a force on the strings connected to it. This force causes all the mesh nodes to move into a new position in order to reach equilibrium again.

Diffusion-based Smoothing A diffusion equation is solved for the mesh displacement velocity: $\nabla \cdot (\gamma \nabla \vec{u}) = 0$. The boundary conditions for $\vec{u}$ are obtained from the boundary movement speed.

The diffusion coefficient is used to control the impact of the boundary's movement on the mesh.

After the diffusion equation is solved the new positions of the nodes are defined as

$$\vec{x}_{new} = \vec{x}_{old} + \vec{u}\Delta t.$$

Using re-meshing was impossible due to its restriction to tetrahedral meshes. Layering works well only for translational movements, especially when the moving boundary is exterior to the computational domain. Therefore the choice was between the two smoothing algorithms. It should be noted however that the latter also fail in case of very strong rotational movement of the boundary, but it was expected that the XT's displacement would not be too large. Otherwise the only option would be to use a tetrahedral mesh and re-meshing.

The diffusion-based smoothing algorithm is said to require more computational effort compared to the string-based, but on the other hand it tends to maintain a better quality mesh. It is also stated that it handles rotation better [7]. Based on these considerations the diffusion-based smoothing algorithms was chosen.

3.8 Initial Conditions

Hybrid initialization was used to obtain an initial distribution of the variables' values in the domain.

The free surface is positioned 1 m below the XT which corresponds to a water depth of 5 meters.

The shape of the surface is set in concordance with the chosen water wave characteristics: amplitude of 1.2 m and wavelength of 30 m. The crest of the wave is positioned at the left boundary of the domain, see figure 3.8.1.

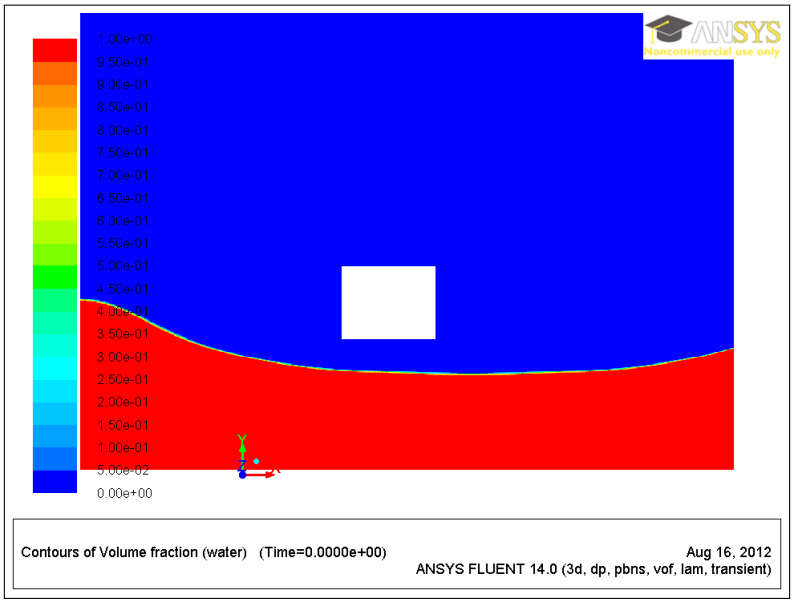

Figure 3.8.1: *Initial disposition of water (red) and air (blue) in the domain.*

3.9 Results

The results for the experiment with the static XT are presented first. Figure 3.9.1 shows the evolution of the x component of the force on the XT. There are two distinct regions where the force is significantly above zero which correspond to two waves hitting the XT.

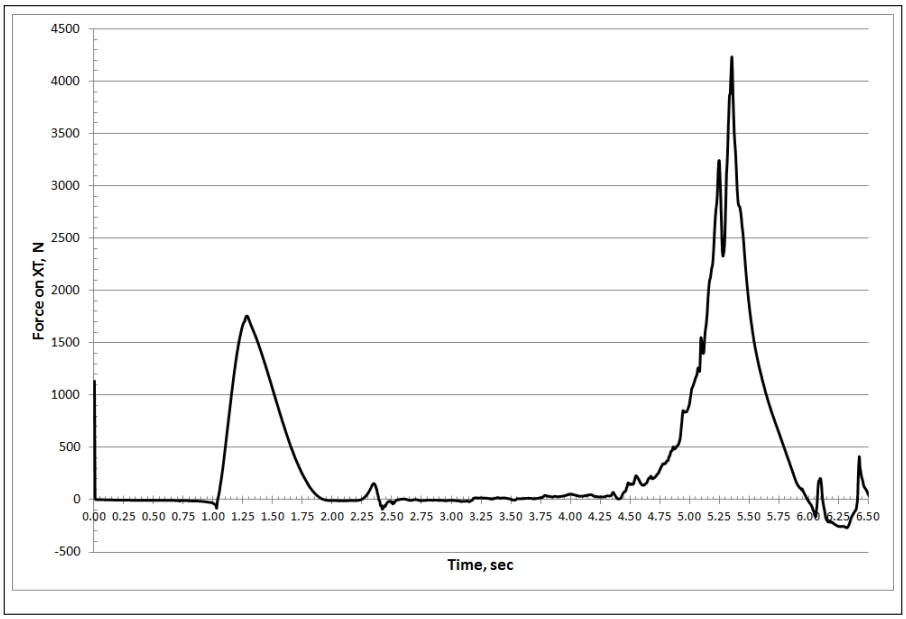

Figure 3.9.1: *The change in the x component of the force acting on the XT in time.*

The first wave is more regular in its form, it is not disturbed on its way towards the XT. This is the reason why the area of the graph corresponding to the first wave is smooth.

Figure 3.9.2 shows the position of the water just prior to the moment where the magnitude of the x component of the force peaks. We see that this moment corresponds to the situation when the water-front has already hit the XT, and some water has begun to move up along the XT's wall, therefore connecting it with the rest of the bulk of water rushing towards it. Afterwords more and more water is redirected upwards by the

XT and the impulse from the wave dies out.

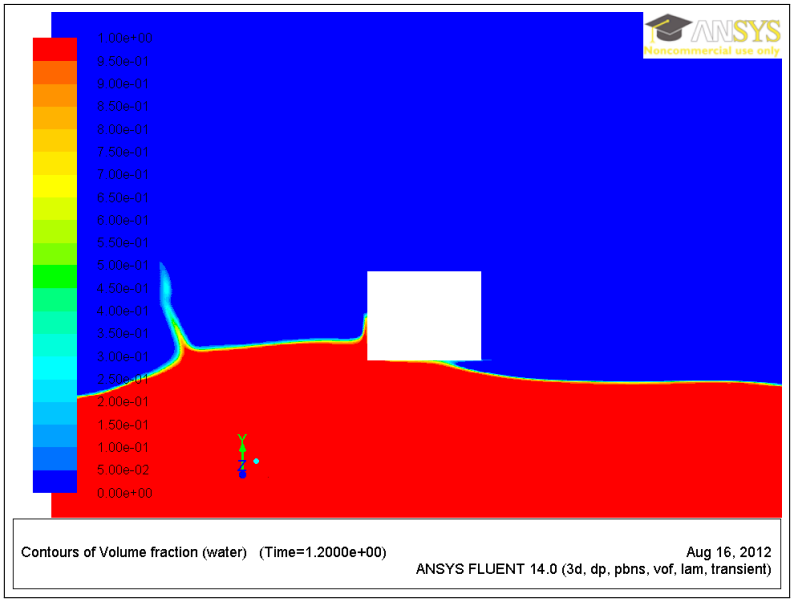

Figure 3.9.2: *Phase distribution near the XT at* $t = 1.20$ *sec.*

We also observe, that the crest of the formed wave is located at around a quarter of the XT's height, which is exactly what was implemented into the wave-generating boundary condition.

After the first wave hits the XT the flow around the XT's vicinity is quite chaotic. The general water level begins to decrease as the wave's trough approaches. The collision causes a small reflection wave to form, resulting in some of the water changing its movement direction towards the inlet. Simultaneously a big bulk continues to flow towards the outlet and under the XT. Also the water that was raised up from the collision begins to fall under the force of gravity. A snapshot of the resulting position of the water is shown on figure 3.9.3.

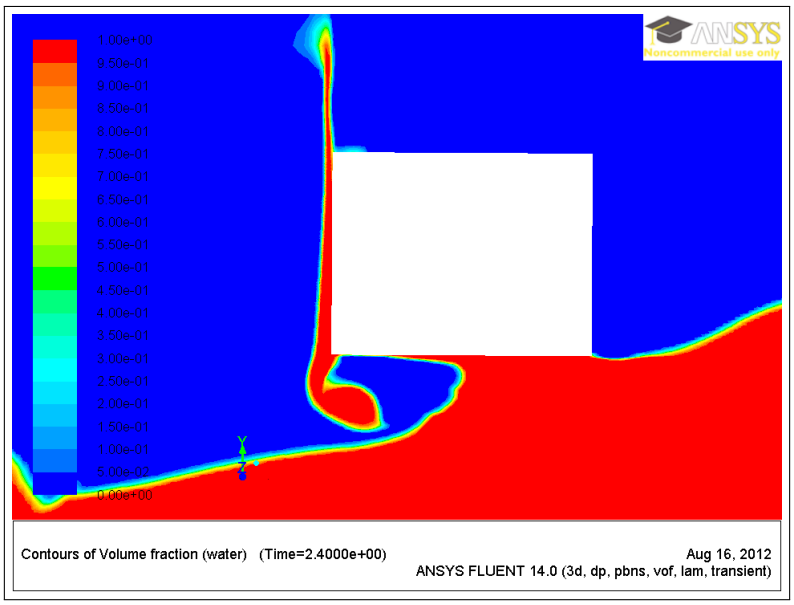

Figure 3.9.3: *Phase distribution near the XT at* $t = 2.40$ *sec.*

The result of this extra chaos is that the second wave manages to gather more water mass as it hits the XT. This results in a force of stronger magnitude on the XT's wall. The more chaotic form of the wave is also

responsible for the oscillations in the force's magnitude. The moment corresponding to the highest value of the x component of the force is shown on figure 3.9.4.

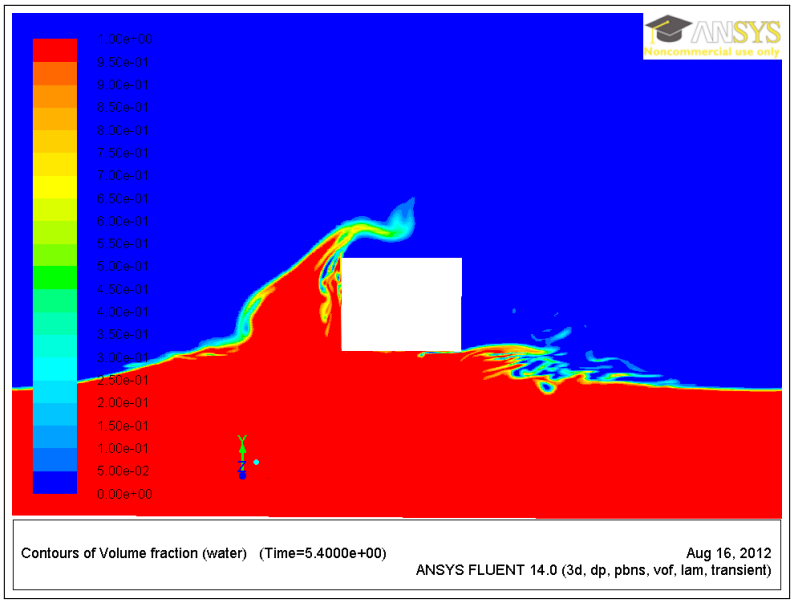

Figure 3.9.4: *Phase distribution near the XT at $t = 5.40$ sec. Corresponds to the second maximum of the x component of the force.*

The graph of the evolution of the y component of the force (figure 3.9.5) is not as intuitive.

The first maximum occurs at the same point in time as that of the x component. The magnitude of the force at this maximum is over two times larger then that of the x component of the force, which is quite peculiar. An explanation for that can be found by observing that figure 3.9.2 indicated that the water from below the XT acts on a significantly larger area. This balances out the lack of momentum in the vertical direction.

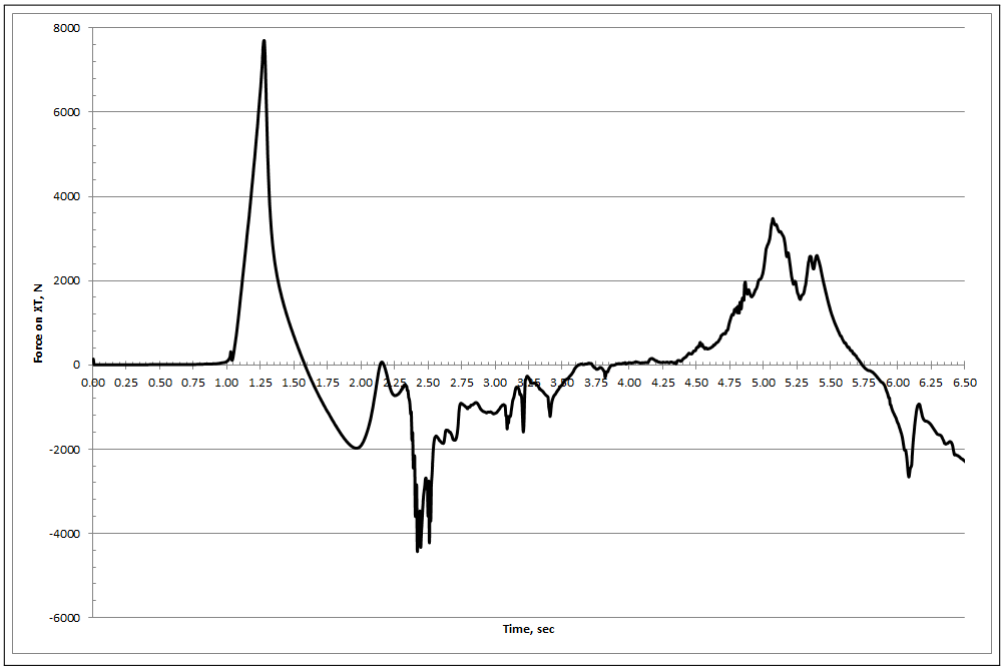

Figure 3.9.5: *The change in the y component of the force acting on the XT in time.*

After the positive impulse dies out irregular negative forces begin to pull the XT down. The magnitude of

these forces are significant, and in order to explain their presence a more careful look at the distribution of flow parameters is required.

Figure 3.9.6 shows the pressure distribution around the XT at the moment when the negative y force is maximum in magnitude. The phase distribution for this moments is shown on figure 3.9.3. A large area with low pressure is visible beneath the XT and a particular small circular area with the lowest pressure is located beneath the XT's edge.

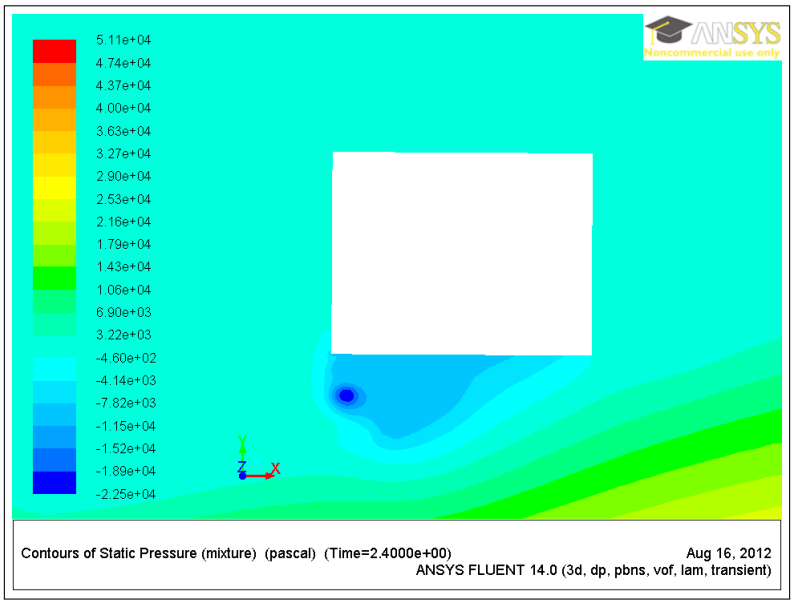

Figure 3.9.6: *Distribution of pressure near the XT at* $t = 2.40$ *sec.*

Figure 3.9.7 shows the velocity vectors in the same region. It is evident that strong recirculation is present near the low-pressure zone.

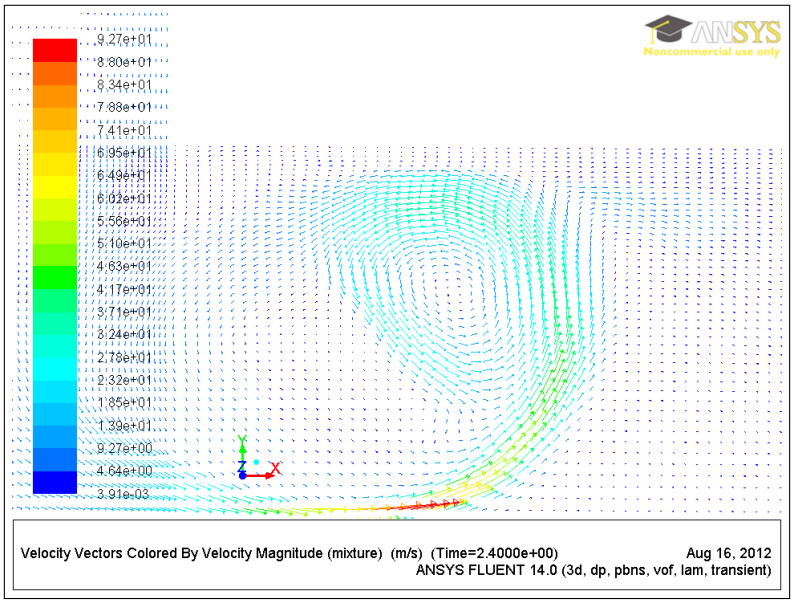

Figure 3.9.7: *Velocity vectors near the low pressure zone beneath the XT at* $t = 2.40$ *sec. Colour corresponds to magnitude.*

There are two causes behind the appearance of these phenomena. The first one is the blockage problem already discussed above. By comparing figure 3.9.7 and 3.9.3 it is seen that the high-velocity and recirculation

zones coincide with the position of the air phase. These high speeds are present because the incoming air goes through a "nozzle" created by the water and then consequently gets blocked by the water as it flows towards the outlet. The high air speeds in turn affect the behaviour of the water.

However the recirculation caused by blockage would not be sufficient to cause such a strong pressure gradient, moreover we observed that the low pressure region still exists when there is only water present below the XT. The reason for that is the sharp rectangular geometry of the XT. The sharp 90 degree angle causes the water rushing down from above along the left wall of the XT to separate, leaving a low-pressure recirculation zone near the lower-left corner. We experienced that with higher velocity waves the pressure can drop low enough for cavitation to begin.

Therefore the conclusion is that the low pressure zone is largely a modelling effect not present in reality and can be removed by improving the geometrical model of the XT.

Finalizing the analysis we want to stress that the force distributions presented here are not necessarily representative for the complex process of the waves-XT interaction. These distribution will change radically depending on the wave parameters, the position of the XT and other modeling parameters. Therefore it is not the results of this particular simulation that are valuable but rather the fact that a framework for conducting and analysing such simulations is built. The conducted simulation therefore plays the role of a proof of concept.

3.9.1 Effect of Fluid-Structure Interaction

Due to the complexity introduced by adding FSI into the model the time-frame of the simulations was shortened to one wave period.

Figure 3.9.8 shows the evolution of the x component of the force for both experiments: with FSI included and without it.

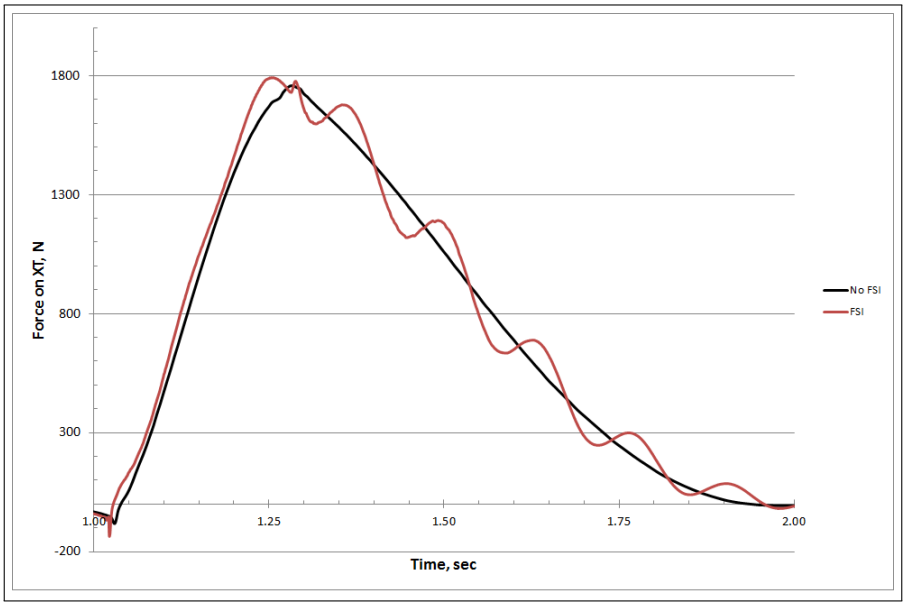

Figure 3.9.8: *The change in the x component of the force acting on the XT in time. FSI included in the model (red) and not (black).*

The figure indicates that FSI introduces regular oscillations into the force's magnitude. However the oscillations only appear after the force has reached its peak. The integral value of the force also stays nearly the same.

Figure 3.9.9 shows the evolution of the force magnitude and the evolution of the maximum deformation of the XT (scaled up).

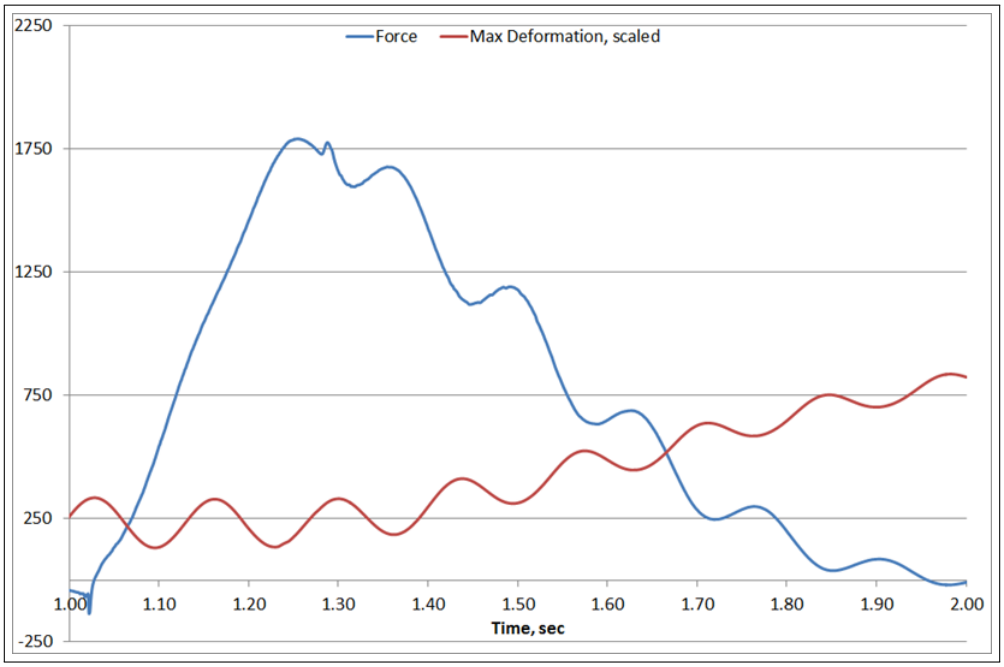

Figure 3.9.9: *The change in the x component of the force acting on the XT (blue) and the scaled maximum deformation of the XT (red).*

Analysing figures 3.9.8 and 3.9.9 allows to describe the process of the FSI. The XT-riser system can be thought of as a pendulum, since the bulk of the mass is concentrated in the XT and the riser is very long compared to the size of the XT. When the wave hits the XT it begins to move to the right, however this does not happen immediately due to the large mass of the XT. Therefore the maximum deformation begins to rise slightly after the force on the XT's wall peak (figure 3.9.9).

As the XT begins to deform it also moves away from the incoming water, so the force magnitude begins to decrease. On the other hand gravity makes the XT go towards the incoming water. As a result the force magnitude oscillates and the local maxima in the force correspond to local minima in the deformation.

It is important to make a conclusion about the necessity of including FSI in the model. The maximum deformation of the XT during the whole simulations did not exceed 0.5 m. Considering the minimal effect the FSI had on the maximum of the force magnitude and the big complexity FSI introduces into the mode,l taking into account is not recommended unless significantly more violent weather regimes are considered.

4 Conclusions

This thesis develops a way to accurately model the behavior of large equipment (the XT) in the sea splash-zone using methods of computational fluid dynamics. The two parts of the thesis deal with two separate problems that need to be resolved for the results of CFD simulations to be meaningful.

The first part is a contribution to the development of an adequate geometrical model of the XT. Instead of introducing a new model, work on a previously proposed model is continued. The objective is to run a CFD simulation to calculate the drag on the model's walls as it is moved through water at constant speed. The results are then to be compared with those obtained experimentally in [1].

The following are the most important results of the conducted work and their implications:

- The values of the drag force's components are calculated for four different flow velocities.
- The accuracy with which these values were calculated is substantial for using them for comparison with further experimental results and for driving further model development.
- The results presented in [1] are highly inaccurate, probably due to problems in the experimental setup.

The second part of the thesis is concentrated on creating a physical and mathematical model of the sea splash-zone and its interaction with the XT. The model is developed using the ANSYS Fluent and Mechanical solvers which implied certain limitations but on the other hand guarantied that the model can be easily set up and adapted to the current needs by anyone with access to these solvers. The latter is important because FMC Technologies' intention is to further use the model for analysing different weather conditions and XT parameters.

The following results were achieved:

- A CFD model suitable for simulating the sea splash-zone at different weather conditions was developed using the ANSYS software package.
- The model allows to account for two-way fluid-structure interaction between the sea waves and the XT. It was concluded however that this interaction can be disregarded for a wide range of weather conditions and XT parameters.
- A detailed analysis of simulation results for a certain configuration of waves and XT parameters was given.

There is a significant amount of possibilities for further development of the models presented in this thesis, both the geometrical and the physical. Currently however the latter can be considered to be developed better.

In order to improve the geometrical model more accurate data about the real XT's parameters needs to be gathered. Once that is obtained a full-scaled iterative process of creating a simpler geometrical alternative can be started, where the current simple designs can be a starting point.

Regarding the physical model of the splash-zone it's performance has to be evaluated for a wider range of weather conditions. Further, the transaction to three-dimensional geometry should be tested.

Bibliography

[1] Stig Kjemperud. **Hydrodynamic Coefficients for Wellhead Structures**. M.Sc. thesis, Norwegian University of Science and Technology, Department of Marine Technology, 2011.

[2] H. K. Versteeg, W. Malalasekera. **An Introduction to Computational Fluid Dynamics: The Finite Volume Method**.

[3] F. R. Menter. **Two-Equation Eddy-Viscosity Turbulence Models for Engineering Applications**. AIAA Journal, 32(8). 1598-1605, August 1994.

[4] D. Quingjie, D. Leung. **2D Numerical Simulation of Ocean Waves**. World Renewable Energy Congress 2011. Sweden, 2011.

[5] K. Jansen, F. Shakib, and T. Hughes. **Computational Nonlinear Mechanics in Aerospace Engineering**. American Institute of Aeronautics and Astronautics, Chapter 5, Fast Projection Algorithm for Unstructured Meshes, 1992

[6] P.F. Galpin, R.B. Broberg, B.R. Hutchinson. Three- Dimensional Navier Stokes **Predictions of Steady-State Rotor/Stator Interaction with Pitch Change**. 3rd Annual Conference of the CFD, Society of Canada, Banff, Alberta, Canada, Advanced Scientific Computing Ltd, June 25-27, 1995

[7] **ANSYS Fluent User Guide**. Release 14, November 2011.

[8] **ANSYS Fluent Theory Guide**. Release 13, November 2010.

5 Appendix

Below the physical dimensions of ModelB are provided. The image is taken from [1]. The inner diameter of the cylinders were disregarded here, since they don't interact with the flow.

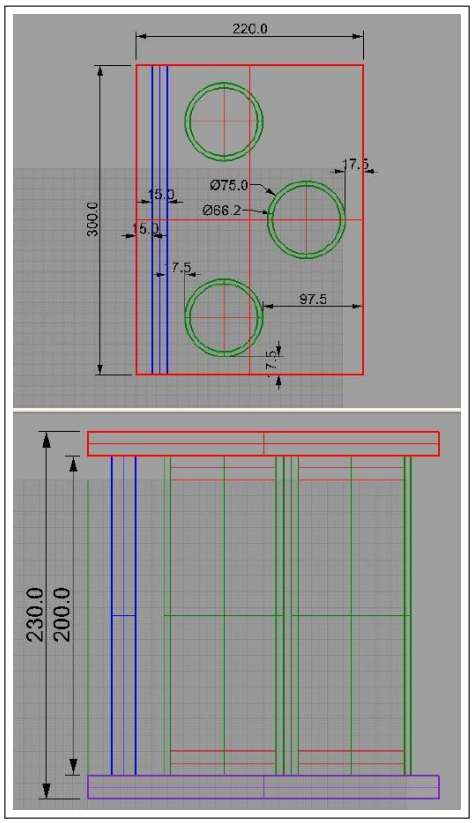

Figure 5.0.1: *ModelB's drawings with dimensions [1].*